Full-scale Microwave SQUID Multiplexer Readout System for Magnetic Microcalorimeters

M. Neidig, T. Muscheid, R. Gartmann, L. E. Ardila Perez, M. Wegner, O. Sander, and S. Kempf

***Abstract*—The deployment of large cryogenic detector arrays, comprising hundreds to thousands of individual detectors, is highly beneficial for various cutting-edge applications, requiring large statistics, angular resolution or imaging capabilities. The readout of such arrays, however, presents a major challenge in terms of system complexity, parasitic heat load, and cost, which can be overcome only through multiplexing. Among the various multiplexing approaches, microwave SQUID multiplexing (μMUXing) currently represents the state of the art, in particular for magnetic microcalorimeter (MMC) readout. In this work, we demonstrate the successful operation of the latest generation of our microwave SQUID multiplexer-based readout system, based on a SQUID multiplexer tailored for MMC readout and a custom full-scale software-defined radio (SDR) electronics, capable of handling up to 400 channels. We operate 14 readout channels simultaneously and demonstrate that the system operates reliably across the entire 4-8 GHz frequency band and achieves low flux white noise levels of $(1.4 \pm 0.2)\,\mu\Phi_0/\sqrt{\mathrm{Hz}}$ in flux-ramp-demodulated readout. While technical steps regarding the SDR output power, as well as a demonstration of the simultaneous readout of the full 400 channels, remain, our results confirm that our system is fully functional and provides a scalable path towards future large-scale, high-resolution MMC experiments.**

***Index Terms*—frequency-division multiplexing, cryogenic radiation detectors, software defined radio, SQUIDs, cryogenic multiplexer**

I. Introduction

Recent advances in state-of-the-art micro- and nanofabrication techniques enable the realization of large-scale cryogenic microcalorimeter arrays comprising thousands of virtually identical detectors. These systems open the path towards next-generation experiments requiring high statistics, angular resolution, or imaging capabilities. The readout of such detector arrays, however, remains challenging due to system complexity, cost, and parasitic heat load, which can typically be addressed only through multiplexing schemes. Resulting requirements are particularly demanding for magnetic microcalorimeter (MMC) arrays [1]–[3], which typically operate at temperatures below $30\,\mathrm{mK}$ and require a signal bandwidth exceeding $\Delta f_{\mathrm{BW}} > 100\,\mathrm{kHz}$. In this context, microwave SQUID multiplexing (μMUXing) [4]–[10] has established itself as the state-of-the-art MMC readout approach. In this scheme, each detector is inductively coupled to a non-hysteretic rf-SQUID, which in turn is coupled to a superconducting microwave resonator with a distinct resonance frequency, coupled to a common feedline. Detector events alter the magnetic flux threading the SQUID loop, thereby modifying its effective inductance and shifting the resonance frequency of the corresponding resonator. This shift is detected by continuously probing the resonator with a microwave carrier and monitoring the amplitude or phase of the transmitted signal. Coupling many such resonators to a single transmission line and using a software-defined radio (SDR) enables simultaneous readout of hundreds of detectors. To linearize the otherwise nonlinear SQUID response, flux-ramp modulation (FRM) is applied [11].

In this work, we report on the performance of the latest generation of our μMUX-based readout system, initially developed for the ECHo experiment [12], which now serves as a general purpose multiplexing platform for MMC based experiments. It features a μMUX specifically optimized for MMC readout and our custom SDR electronics [13]–[15]. For the first time, we employ a fully equipped and configured version of this SDR electronics, capable of reading out 400 multiplexer channels in $4\text{-}8\,\mathrm{GHz}$ frequency band. For performance benchmarking, we used an MMC array, originally designed for radionuclide metrology [16]. We integrated both MMC array and μMUX into a custom detector setup, and investigated the performance of the full readout chain across the complete frequency band.

II. μMUX Description

We designed and fabricated a dedicated μMUX chip on a thermally oxidized Si substrate, using Josephson tunnel junctions based on a Nb/Al–AlO_x/Nb trilayer. The resonators are defined in the bottom Nb layer of the trilayer. The chip was developed to evaluate the SDR system across its full bandwidth from $4\,\mathrm{GHz}$ to $8\,\mathrm{GHz}$. It comprises eighteen coplanar waveguide (CPW) superconducting quarter-wave resonators, each capacitively coupled to a common CPW feedline. The opposite end of each resonator is terminated by a load inductor that is inductively coupled to an rf-SQUID (see Fig. 1(c) and (e)). The resonator lengths were chosen to yield resonance frequencies between $4.25\,\mathrm{GHz}$ and $7.75\,\mathrm{GHz}$, with frequency spacings ranging from $10\,\mathrm{MHz}$ to $500\,\mathrm{MHz}$. This design ensured coverage of the full frequency band while also testing the target μMUX channel spacing of $10\,\mathrm{MHz}$. The resulting

M. Neidig is with the Institute of Micro- and Nanoelectronic Systems, Karlsruhe Institute of Technology, 76187 Karlsruhe, Germany (e-mail: martin.neidig@kit.edu).

T. Muscheid, R. Gartmann, L. E. Ardila Perez, and O. Sander are with the Institute for Data Processing and Electronics, Karlsruhe Institute of Technology, 76344 Eggenstein-Leopoldshafen, Germany.

M. Wegner is with with the Institute for Data Processing and Electronics, Karlsruhe Institute of Technology, 76344 Eggenstein-Leopoldshafen, Germany, and also with the Institute of Micro- and Nanoelectronic Systems, Karlsruhe Institute of Technology, 76187 Karlsruhe, Germany.

S. Kempf is with the Institute of Micro- and Nanoelectronic Systems, Karlsruhe Institute of Technology, 76187 Karlsruhe, Germany, and also with the Institute for Data Processing and Electronics, Karlsruhe Institute of Technology, 76344 Eggenstein-Leopoldshafen, Germany (e-mail: sebastian.kempf@kit.edu).

This article has been accepted for publication in IEEE Transactions on Applied Superconductivity. This is the author's version which has not been fully edited and content may change prior to final publication. Citation information: DOI 10.1109/TASC.2026.3696057

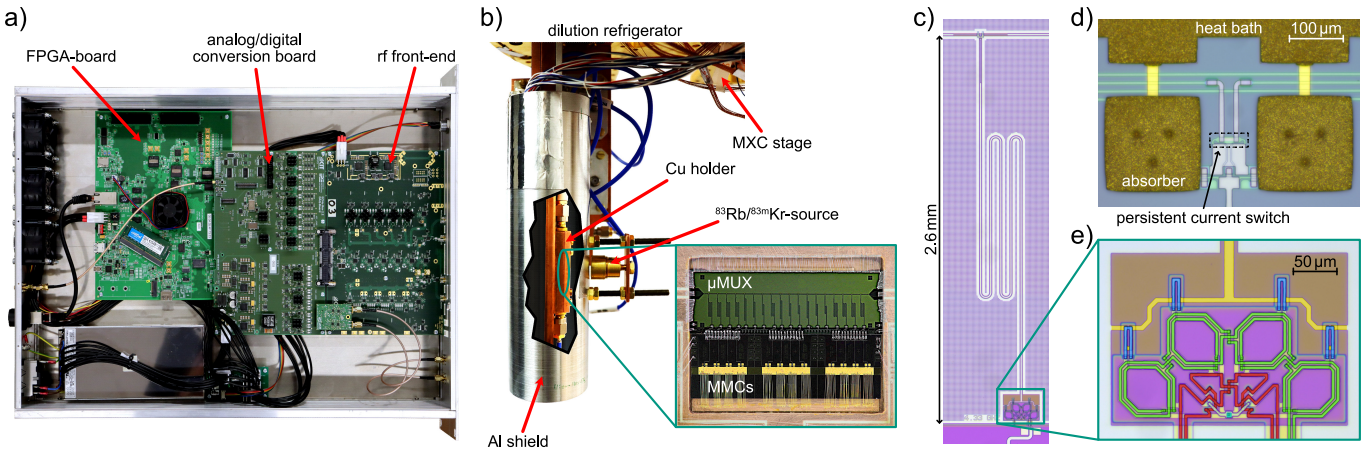

Fig. 1. (a) Photograph of the custom full-stack ECHo DAQ SDR electronics inside an aluminum housing. The system comprises a digital processing board, an analog/digital conversion board, and a high-frequency analog heterodyne mixer board. (b) Photograph of the experimental setup, mounted on the mixing chamber (MXC) platform of the ^{3}He/^{4}He dilution refrigerator. The μMUX and MMC array are enclosed in a common copper housing and shielded from external magnetic field fluctuations by a superconducting aluminum shield. A small aperture in the shield permits radiation to reach the detector. The ^{83}Rb/^{83m}Kr source used for event generation is mounted outside the shield, close to the aperture. A series of collimators ensures that only X-rays from the source reach the detectors. (c) Micrograph of a μMUX channel with a resonance frequency of 4.362 GHz. The channel consists of a CPW quarter-wavelength resonator, capacitively coupled to the feedline at the top and terminated at the bottom with an inductor that is inductively coupled to an rf-SQUID. (d) Micrograph of a two-pixel detector from the MMC array. Beneath the free-standing gold absorber are the paramagnetic sensor and the superconducting pickup coil, as described in [3]. (e) Enlarged view of the rf-SQUID of the μMUX channel shown in (c). The Josephson tunnel junction is highlighted in turquoise, the modulation coil in red, the input coil in green, and the CPW resonator's terminating inductor in yellow. The coupling between the rf-SQUID and the terminating inductor is set by the length of the inductors highlighted in blue.

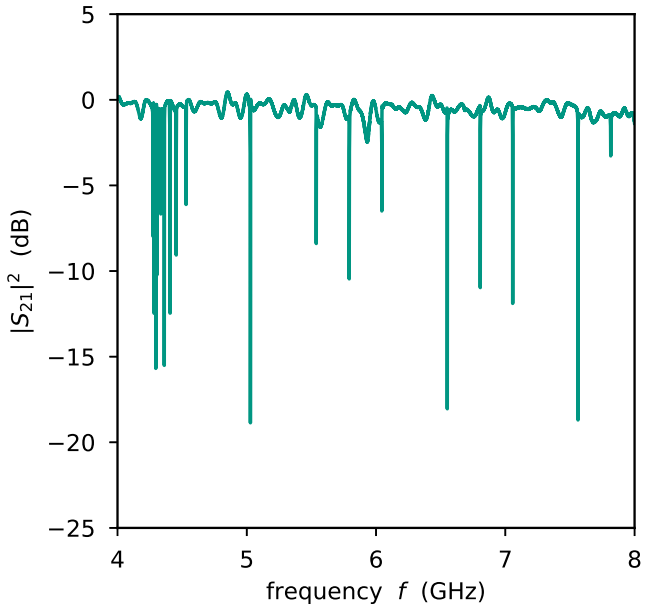

Fig. 2. Measured μMUX transmission $|S_{21}|^2$ across the full frequency band, recorded at $T < 7\,\mathrm{mK}$ and using a VNA output power of $P_{\mathrm{VNA}} = -25\,\mathrm{dBm}$ corresponding to an on chip power of $P_{\mathrm{chip}} \approx -68\,\mathrm{dBm}$. A cryogenic rf switch enabled calibration measurements through the same wiring while bypassing the μMUX, allowing normalization of the measured $|S_{21}|^2$ curve.

transmission spectrum is shown in Fig. 2. While this configuration demonstrates that our μMUX design facilitates a 10 MHz in the low 4 GHz range, an investigation of the achievable homogeneity of the resonance frequency spacing across the entire frequency range from $4 - 8\,\mathrm{GHz}$ has not yet been carried out. The coupling capacitors were designed to provide a resonator bandwidth of 1 MHz, assuming negligible internal resonator losses. The coupling between the resonator and rf-SQUID was varied between 2.8 pH and 5.3 pH, depending on frequency, to achieve a peak-to-peak frequency shift of 2 MHz for each resonator, thereby minimizing flux noise [17]. The non-hysteretic rf-SQUIDs were designed with a screening parameter of $\beta_{\mathrm{L}} = 2\pi L_{\mathrm{S}} I_{\mathrm{c}}/\Phi_0 = 0.6$, corresponding to a critical current of $I_{\mathrm{c}} = 4.8\,\mu\mathrm{A}$ for an rf-SQUID inductance of $L_{\mathrm{S}} = 41\,\mathrm{pH}$. The μMUX pad layout was made compatible with the employed MMC array [16]. However, the rf-SQUID input inductance of $L_{\mathrm{in}} = 1.4\,\mathrm{nH}$ introduces a slight impedance mismatch between the μMUX and the detector. Assuming a parasitic inductance of $L_{\mathrm{par}} = 0.25\,\mathrm{nH}$ due to the wiring connecting the MMC and the μMUX, the optimal input inductance would be 0.81 nH. This mismatch leads to a reduction of the signal amplitudes generated by the MMC in the input coil by less than 5 % and therefore only weakly impacts the achievable energy resolution of the system. To suppress microwave leakage from the resonators into the detector, a $5\,\Omega$ shunt resistor was placed in parallel with the input coil, forming a first-order LR low-pass filter. To avoid distributed-circuit behavior, the resistor was placed in close proximity to the rf-SQUID input coil.

III. SDR System Description

Room-temperature control and readout of the μMUX is provided by custom SDR-based DAQ electronics [15]. The hardware and firmware of this system are optimized for MMC readout and cover the 4-8 GHz band. As shown in Fig. 1(a), the system consists of three distinct boards: an analog rf front-end, an analog/digital conversion board, and an

FPGA board for digital signal processing. The analog front-end includes two-stage mixers that convert the 4 GHz wide signal into five baseband signals, each with 800 MHz complex bandwidth [14]. These baseband signals are subsequently digitized by dual-channel ADCs operating at 1 GSPS and processed in real-time by a processing chain implemented in the programmable logic of an AMD MPSoC. The transmission side of the DAQ system, used for resonator excitation, is constructed analogously, employing three four-channel DACs with 1 GSPS. Two additional DACs generate the sawtooth flux signal required for FRM.

The FPGA firmware contains several stages of real-time signal processing. First, frequency demultiplexing is performed to separate individual μMUX channels, using a digital down-conversion (DDC) stage with a polyphase channelizer and a filterbank [15] designed for the target 10 MHz channel spacing. Subsequently, each channel is FRM-demodulated to reconstruct the raw detector signal, with the mixing frequency independently adjustable according to the specific SQUID response. Finally, a trigger extracts detector signals, pre-trigger samples, and metadata such as a timestamp and the channel index. All modules of the processing chain can be configured at runtime to meet the experiment's requirements. Data (raw, FRM-demodulated, triggered) can be acquired in snapshot or continuous mode and transferred via Ethernet to a control PC for offline post-processing.

IV. Experimental Setup

The MMC array was mounted close to the μMUX inside a copper enclosure (see Fig. 1(b)). The array is identical to the implanted ^{55}Fe chip described in [16], but without ^{55}Fe implantation. Instead, an external ^{83}Rb/^{83m}Kr source was used to generate detector signals. The array comprises twelve two-pixel detectors (see Fig. 1(d)), eight of which were functional. On the μMUX side, three of eighteen channels didn't show a resonance shift due to a short in the modulation line, and one resonance was too shallow to provide sufficient amplitude for FRM. As a result, 14 μMUX channels were usable, seven of which were connected to an MMC.

The sample holder was mounted on the mixing chamber stage of a ^{3}He/^{4}He dilution refrigerator with pulse-tube pre-cooling, reaching a base temperature below 7 mK. To shield the setup from external magnetic field fluctuations, the sample holder was enclosed in a superconducting aluminum shield. The ^{83}Rb/^{83m}Kr source was mounted outside the shield, with the emitted X-rays directed onto the MMC absorbers through a sequence of apertures in the aluminum shield and sample holder. To ensure that only MMC absorbers were irradiated, a collimator was glued onto the slit in the copper holder. The final collimator, a Si chip patterned by deep reactive-ion etching, contains several $150\,\mu\text{m} \times 150\,\mu\text{m}$ apertures positioned directly above the MMC absorbers. Since ^{83m}Kr emits both electrons and X-ray photons, the slit in the aluminum shield was covered by a $\sim 20\,\mu\text{m}$ thick aluminum foil that blocked electrons while transmitting most X-rays.

The SDR electronics outside the cryostat were connected to the μMUX via a chain of flexible and semi-rigid coaxial cables. The multiplexer input line was attenuated by about 43 dB using cryogenic attenuators and a directional coupler, all thermally anchored at different cryostat stages. On the receiver side, the signal was first amplified at 4 K with a cryogenic high-gain, ultra-low-noise HEMT amplifier, followed by an additional amplifier at room temperature.

V. System Characterization

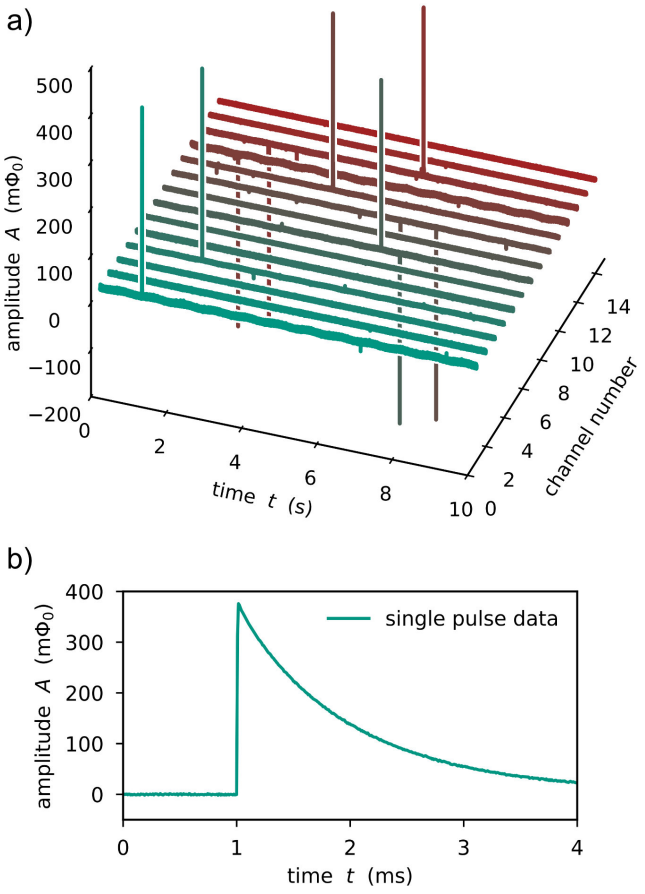

Fig. 3. (a) FRM-demodulated time-stream data of 14 simultaneously operated μMUX readout channels. Seven channels are connected to two-pixel MMCs and exhibit detector signals appearing as spikes in the time stream. The pixels of each MMC can be distinguished by the signal polarity. (b) Zoom into one of the acquired detector signals, showing the expected exponential decay.

Basic μMUX characteristics were determined by measuring the transmission parameter $|S_{21}|^2$ (see Fig. 2) at different constant flux offsets, provided by a dc current through the modulation line. For FRM, a sawtooth signal with an amplitude of $3.8\,\Phi_0$ and a repetition rate of 122 kHz was applied through the modulation line. After removing the transient regions at the beginning and end of each ramp segment, an effective signal amplitude of $3\,\Phi_0$ remained and was used for demodulation, following the method described in [11]. While the system is capable of FRM repetition rates up to 1.9 MHz, we chose 122 kHz due to the limited bandwidth of our cryostats modulation line wiring. This choice also enables comparison with measurements performed using a previous iteration of the SDR system [18], [19].

Detector events were recorded at $T < 7\,\mathrm{mK}$, while noise spectra were acquired at $T = 600\,\mathrm{mK}$ to suppress MMC detector signals. Only the noise contribution from thermodynamic energy fluctuations (TEF) in the MMC is suppressed along with the MMC signals at this elevated temperature. However, the TEF noise is dominated by the contributions from the HEMT amplifier and room temperature electronics, which are independent of the mixing chamber temperature. Other noise contributions, such as erbium spin noise, remain temperature independent [20] or increase with temperature, as is the case with Johnson noise contributions from both the filter resistor and the normal conducting sensor material. Consequently, the noise performance measured at $600,\mathrm{mK}$ represents an upper limit on the achievable system noise at base temperature.

For each μMUX channel, the frequency and amplitude of the microwave readout tone were optimized to minimize the FRM-demodulated flux noise. First, we measured the flux noise of each channel for multiple carrier frequencies around the resonance. At the frequency yielding the lowest noise, we repeated the measurement for several tone power levels. This procedure provided the final readout tone parameters.

Figure 3(a) shows time-stream data simultaneously acquired from 14 μMUX channels over a duration of $10\,\mathrm{s}$. A zoomed-in view of a single detector event in channel 10, operated with a microwave carrier of $4.455\,\mathrm{GHz}$, is displayed in Fig.3(b). The signals exhibit the expected exponential decay with a decay time of $1.1\,\mathrm{ms}$, consistent with results obtained using a two-stage dc-SQUID setup [16], [21]. In contrast, the rise time was not evaluated, since the sampling rate set by the FRM repetition rate did not provide sufficient resolution in this measurement.

The SDR system has been successfully operated with the target value of 400 readout tones. At cryogenic temperature, however, only 14 μMUX channels were available for simultaneous readout. In addition, the DAC output power, combined with the installed attenuation in the cryogenic input line, proved insufficient to provide the optimal readout power for all 400 channels. Future experiments will therefore require either an amplifier at the SDR output or reduced attenuation in the cryogenic input line.

Fig. 4 shows results from flux noise measurements, recorded with the readout system at a mixing chamber temperature of $600\,\mathrm{mK}$. Initial tests indicated that the SDR system primarily limited the noise performance. However, we could mitigate this limitation by adding a low-noise amplifier at the SDR input. Fig. 4(a) presents a resulting open-loop flux-noise spectrum of one μMUX channel. The output of the digital down-conversion stage in the SDR electronics was first measured as a function of magnetic flux applied through the rf-SQUID modulation coil. From this response, we determined the flux bias corresponding to maximum sensitivity and extracted the transfer coefficient between the DDC signal and magnetic flux. We then calculated the noise spectrum from one million samples acquired at a sampling rate of $15.625\,\mathrm{MHz}$, with the μMUX biased at maximum sensitivity. Equivalent measurements were performed for all 14 μMUX channels. To further assess the noise performance under detector operation, we also recorded noise traces during FRM-demodulated readout. Fig. 4(b) presents an example FRM–demodulated noise spectrum of a single μMUX channel. Although the spectrum contains several parasitic noise contributions, the channel nevertheless exhibits a very low white-noise level of $\sqrt{S_{\Phi,\mathrm{FRM,white}}} = 1.26\,\mu\Phi_0/\sqrt{\mathrm{Hz}}$.

We observed excellent noise performance across all measured μMUX channels. Fig. 4(c) presents the white noise level of all active μMUX channels, measured in both open-loop and FRM–modulated operation. In open-loop mode, the white noise level consistently remained below $1\,\mu\Phi_0/\sqrt{\mathrm{Hz}}$ across the full 4-$8\,\mathrm{GHz}$ band, with a mean value of $(0.7 \pm 0.1)\,\mu\Phi_0/\sqrt{\mathrm{Hz}}$. With FRM, the white noise increased to $(1.4 \pm 0.2)\,\mu\Phi_0/\sqrt{\mathrm{Hz}}$. This increase is consistent with the $\sqrt{2/\alpha}$ factor (with $\alpha \approx 0.8$, the fraction of the flux ramp used for demodulation) [11] and the non-ideal sinusoidal modulation of the readout tone amplitude [17]. Notably, the demodulated noise spectra consistently yielded noise levels below $2\,\mu\Phi_0/\sqrt{\mathrm{Hz}}$. The single outlier at $6\,\mathrm{GHz}$ was traced to an incorrect demodulation frequency setting and was hence excluded from the calculation of the mean noise performance. When expressed in terms of current noise, the present system achieves a noise level of $(19 \pm 3)\,\mathrm{pA}/\sqrt{\mathrm{Hz}}$, comparable to state-of-the-art μMUX devices optimized for TES readout [22]–[24]. However, the noise performance of different μMUX devices is not directly comparable because the SQUID and input coil inductances vary between designs. A more suitable figure of merit is therefore the intrinsic SQUID energy sensitivity $\epsilon = S_\Phi/(2L_\mathrm{S})$ and the input-referred coupled energy sensitivity $\epsilon_\mathrm{c} = \epsilon/k_\mathrm{in}^2$, where k_in denotes the magnetic coupling factor between the SQUID loop and the input coil. Using this metric, our μMUX system achieves $\epsilon = 158\,h$ and $\epsilon_\mathrm{c} = 374\,h$, corresponding to a $\sim$ 3-fold improvement in energy sensitivity over the previous SDR iteration [18], [19] and a factor of only ~ 3.5 degradation in the achievable energy resolution of an optimized MMC compared to an ideal quantum-limited readout [3], [25].

We observe no difference in the noise performance between channels connected to MMCs and those without, indicating that at $600\,\mathrm{mK}$ either the μMUX or the SDR electronics dominates the overall white noise level, and that microwave power leakage into the MMCs is likely small and does not affect the systems noise performance. However, the impact of microwave power leakage on the MMC signals and the achievable energy resolution at base temperature was not investigated in this work. Furthermore, no correlation was found between the intrinsic quality factor of the channels and their individual noise levels, indicating that losses in the resonators do not limit the noise performance, as seen for earlier devices [19]. These results confirm that the multiplexed readout achieves consistently excellent noise performance across all channels, demonstrating that the presented readout system is well suited for high-resolution, large-scale MMC experiments.

VI. Conclusion

We have demonstrated the successful operation of our latest-generation μMUX-based readout system for MMC readout,

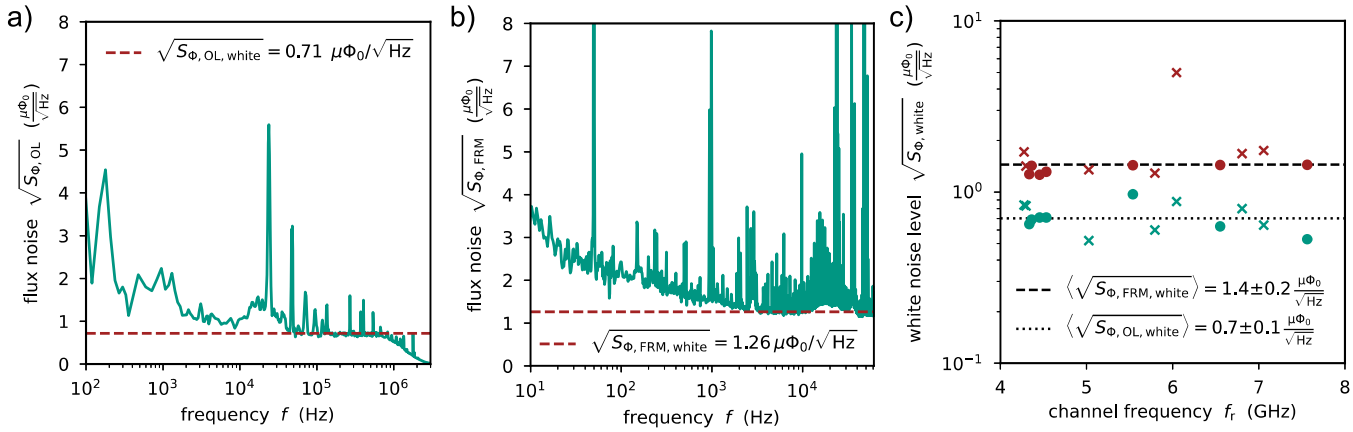

Fig. 4. Flux-noise measurements of the fully operational readout system with the μMUX operated at 600 mK. (a) Example open-loop flux-noise spectrum of the μMUX channel, operated with a microwave carrier of 4.455 GHz. A constant current in the modulation line biases the rf-SQUID for maximum sensitivity. (b) Example FRM–modulated flux noise spectrum of the same μMUX channel. (c) White noise level of all operated μMUX channels plotted against channel frequency. Circles indicate channels with functional MMCs connected, while crosses denote channels without detectors. Green data correspond to open-loop measurements, and red data correspond to FRM–modulated measurements.

for the first time capable of handling up to 400 detectors. The system operates reliably across the full 4–8 GHz band and achieves white noise levels of about $1.4\,\mu\Phi_0/\sqrt{\text{Hz}}$ in FRM–demodulated readout. Notably, no degradation in noise performance was observed for channels connected to detectors, indicating that potential microwave power leakage into the MMC sensor is negligible. While technical challenges regarding the SDR output power and the demonstration of consistent μMUX channel parameters across the full 4-8 GHz frequency band remain, these results confirm that our SDR-based multiplexed readout is fully functional and provide a solid foundation for future large-scale, high-resolution MMC experiments.

Acknowledgment

M. Neidig, T. Muscheid, and R. Gartmann gratefully acknowledge support from the Karlsruhe School of Elementary Particle and Astroparticle Physics: Science and Technology (KSETA). This work was partially funded by the Deutsche Forschungsgemeinschaft (DFG, German Research Foundation) – Projektnummer (project number) 467785074.

References

[1] A. Fleischmann, C. Enss, and G. Seidel, *Metallic Magnetic Calorimeters*. Springer Berlin Heidelberg, 2005, pp. 151–216. [Online]. Available: https://doi.org/10.1007/b12169

[2] S. R. Bandler, K. D. Irwin, D. Kelly, P. N. Nagler, J.-P. Porst, H. Rotzinger, J. E. Sadleir, G. M. Seidel, S. J. Smith, and T. R. Stevenson, "Magnetically coupled microcalorimeters," *J. Low Temp. Phys.*, vol. 167, no. 3-4, pp. 254–268, May 2012. [Online]. Available: https://doi.org/10.1007/s10909-012-0544-4

[3] S. Kempf, A. Fleischmann, L. Gastaldo, and C. Enss, "Physics and applications of metallic magnetic calorimeters," *J. Low Temp. Phys.*, vol. 193, no. 3-4, pp. 365–379, 2018. [Online]. Available: https://doi.org/10.1007/s10909-018-1891-6

[4] K. D. Irwin and K. W. Lehnert, "Microwave squid multiplexer," *Applied Physics Letters*, vol. 85, no. 11, pp. 2107–2109, 2004. [Online]. Available: https://doi.org/10.1063/1.1791733

[5] J. A. B. Mates, G. C. Hilton, K. D. Irwin, L. R. Vale, and K. W. Lehnert, "Demonstration of a multiplexer of dissipationless superconducting quantum interference devices," *Applied Physics Letters*, vol. 92, 2008. [Online]. Available: https://doi.org/10.1063/1.2803852

[6] S. Kohjiro, F. Hirayama, H. Yamamori, S. Nagasawa, D. Fukuda, and M. Hidaka, "White noise of nb-based microwave superconducting quantum interference device multiplexers with nbn coplanar resonators for readout of transition edge sensors," *Journal of Applied Physics*, vol. 115, no. 22, 2014. [Online]. Available: https://doi.org/10.1063/1.4882118

[7] S. Kempf, M. Wegner, L. Deeg, A. Fleischmann, L. Gastaldo, F. Herrmann, D. Richter, and C. Enss, "Design, fabrication and characterization of a 64 pixel metallic magnetic calorimeter array with integrated, on-chip microwave squid multiplexer," *Superconductor Science and Technology*, vol. 30, no. 6, p. 065002, may 2017. [Online]. Available: https://dx.doi.org/10.1088/1361-6668/aa6d17

[8] S. Kempf, M. Wegner, A. Fleischmann, L. Gastaldo, F. Herrmann, M. Papst, D. Richter, and C. Enss, "Demonstration of a scalable frequency-domain readout of metallic magnetic calorimeters by means of a microwave SQUID multiplexer," *AIP Adv.*, vol. 7, no. 1, p. 015007, Jan. 2017. [Online]. Available: https://doi.org/10.1063/1.4973872

[9] B. Dober, Z. Ahmed, K. Arnold, D. T. Becker, D. A. Bennett, J. A. Connors, A. Cukierman, J. M. D'Ewart, S. M. Duff, J. E. Dusatko, J. C. Frisch, J. D. Gard, S. W. Henderson, R. Herbst, G. C. Hilton, J. Hubmayr, Y. Li, J. A. B. Mates, H. McCarrick, C. D. Reintsema, M. Silva-Feaver, L. Ruckman, J. N. Ullom, L. R. Vale, D. D. Van Winkle, J. Vasquez, Y. Wang, E. Young, C. Yu, and K. Zheng, "A microwave SQUID multiplexer optimized for bolometric applications," *Appl. Phys. Lett.*, vol. 118, no. 6, p. 062601, Feb. 2021. [Online]. Available: https://doi.org/10.1063/5.0033416

[10] M. Schmelz, E. Heinz, K. Peiselt, G. Zieger, O. Brandel, D. Born, J. Kunert, M. Siegel, V. Zakosarenko, M. Meyer, and R. Stolz, "Scalable microwave squid multiplexer readout architecture for tes-based thz security camera," *IEEE Transactions on Applied Superconductivity*, vol. 35, no. 3, pp. 1–5, 2025. [Online]. Available: https://doi.org/10.1109/TASC.2025.3545212

[11] J. A. B. Mates, K. D. Irwin, L. R. Vale, G. C. Hilton, J. Gao, and K. W. Lehnert, "Flux-ramp modulation for squid multiplexing," *Journal of Low Temperature Physics*, vol. 167, no. 5-6, pp. 707–712, 2012. [Online]. Available: https://doi.org/10.1007/s10909-012-0518-6

[12] L. Gastaldo, K. Blaum, K. Chrysalidis, T. Day Goodacre, A. Domula, M. Door, H. Dorrer, C. E. Düllmann, K. Eberhardt, S. Eliseev, C. Enss, A. Faessler, P. Filianin, A. Fleischmann, D. Fonnesu, L. Gamer, R. Haas, C. Hassel, D. Hengstler, J. Jochum, K. Johnston, U. Kebschull, S. Kempf, T. Kieck, U. Köster, S. Lahiri, M. Maiti, F. Mantegazzini, B. Marsh, P. Neroutsos, Y. N. Novikov, P. C. O. Ranitzsch, S. Rothe, A. Rischka, A. Saenz, O. Sander, F. Schneider, S. Scholl, R. X. Schüssler, C. Schweiger, F. Simkovic, T. Stora, Z. Szücs, A. Türler, M. Veinhard, M. Weber, M. Wegner, K. Wendt, and K. Zuber, "The electron capture in 163ho experiment – ECHo," *Eur. Phys. J. Spec. Top.*, vol. 226, no. 8, pp. 1623–1694, Jun. 2017. [Online]. Available: https://doi.org/10.1140/epjst/e2017-70071-y

[13] O. Sander, N. Karcher, O. Kromer, S. Kempf, M. Wegner, C. Enss,

and M. Weber, "Software-defined radio readout system for the ECHo experiment," *IEEE Trans. Nucl. Sci.*, vol. 66, no. 7, pp. 1204–1209, Jul. 2019. [Online]. Available: https://doi.org/10.1109/TNS.2019.2914665

[14] R. Gartmann, N. Karcher, R. Gebauer, O. Krömer, and O. Sander, "Progress of the echo sdr readout hardware for multiplexed mmcs," *Journal of Low Temperature Physics*, vol. 209, pp. 726–733, 2022. [Online]. Available: https://doi.org/10.1007/s10909-022-02854-1

[15] T. Muscheid, R. Gartmann, N. Karcher, F. Schuderer, M. Neidig, M. Balzer, L. E. Ardila-Perez, S. Kempf, and O. Sander, "Full-scale readout electronics for the echo experiment," *Journal of Low Temperature Physics*, vol. 217, pp. 456–463, 2024. [Online]. Available: https://doi.org/10.1007/s10909-024-03213-y

[16] M. Müller, M. Rodrigues, J. Beyer, M. Loidl, and S. Kempf, "Magnetic microcalorimeters for primary activity standardization within the empir project prima-ltd," *Journal of Low Temperature Physics*, vol. 214, pp. 263–271, 2024. [Online]. Available: https://doi.org/10.1007/s10909-024-03048-7

[17] C. Schuster, M. Wegner, and S. Kempf, "Simulation framework for microwave squid multiplexer optimization," *Journal of Applied Physics*, vol. 133, no. 4, p. 044503, 01 2023. [Online]. Available: https://doi.org/10.1063/5.0135124

[18] D. Richter, "Multikanal-auslesung von metallischen magnetischen kalorimetern mittels eines vollständigen mikrowellen-squid-multiplexer-systems," Ph.D. dissertation, Heidelberg University, 2021. [Online]. Available: https://doi.org/10.11588/heidok.00030266

[19] D. Richter, M. Wegner, F. Ahrens, C. Enss, N. Karcher, O. Sander, C. Schuster, M. Weber, T. Wolber, and S. Kempf, "Simultaneous mmc readout using a tailored μmux based readout system," *IEEE Transactions on Applied Superconductivity*, vol. 33, no. 5, pp. 1–5, 2023. [Online]. Available: https://doi.org/10.1109/TASC.2023.3264200

[20] A. Fleischmann, M. Link, T. Daniyarov, H. Rotzinger, C. Enss, and G. M. Seidel, "Metallic magnetic calorimeters (MMC): detectors for high-resolution x-ray spectroscopy," *Nucl. Instrum. Methods Phys. Res. A*, vol. 520, no. 1-3, pp. 27–31, Mar. 2004. [Online]. Available: https://doi.org/10.1016/j.nima.2003.11.212

[21] M. Müller, "Magnetische mikrokalorimeter für die aktivitätsstandardisierung und die messung fundamentaler zerfallsdaten in der radionuklidmetrologie," Ph.D. dissertation, Karlsruhe Institute of Technology, 2025. [Online]. Available: https://doi.org/10.5445/IR/1000181097

[22] D. A. Bennett, J. A. B. Mates, S. R. Bandler, D. T. Becker, J. W. Fowler, J. D. Gard, G. C. Hilton, K. D. Irwin, K. M. Morgan, C. D. Reintsema, K. Sakai, D. R. Schmidt, S. J. Smith, D. S. Swetz, J. N. Ullom, L. R. Vale, and A. L. Wessels, "Microwave SQUID multiplexing for the lynx x-ray microcalorimeter," *J. Astron. Telesc. Instrum. Syst.*, vol. 5, no. 02, p. 1, Mar. 2019. [Online]. Available: https://doi.org/10.1117/1.JATIS.5.2.021007

[23] Y. Nakashima, F. Hirayama, S. Kohjiro, H. Yamamori, S. Nagasawa, A. Sato, S. Yamada, R. Hayakawa, N. Y. Yamasaki, K. Mitsuda, K. Nagayoshi, H. Akamatsu, L. Gottardi, E. Taralli, M. P. Bruijn, M. L. Ridder, J. R. Gao, and J. W. A. den Herder, "Low-noise microwave SQUID multiplexed readout of 38 x-ray transition-edge sensor microcalorimeters," *Appl. Phys. Lett.*, vol. 117, no. 12, Sep. 2020. [Online]. Available: https://doi.org/10.1063/5.0016333

[24] J. C. Groh, Z. Ahmed, J. Austermann, J. Beall, D. Daniel, S. M. Duff, S. W. Henderson, J. Hubmayr, R. Lew, M. Link, T. J. Lucas, J. A. B. Mates, M. Silva-Feaver, R. Singh, J. Ullom, L. Vale, J. Van Lanen, M. Vissers, and C. Yu, "Demonstration of a 1820 channel multiplexer for transition-edge sensor bolometers," *Appl. Phys. Lett.*, vol. 127, no. 15, Oct. 2025. [Online]. Available: https://doi.org/10.1063/5.0290914

[25] S. Kempf, A. Ferring, A. Fleischmann, and C. Enss, "Direct-current superconducting quantum interference devices for the readout of metallic magnetic calorimeters," *Supercond. Sci. Technol.*, vol. 28, no. 4, p. 045008, Apr. 2015. [Online]. Available: https://doi.org/10.1088/0953-2048/28/4/045008